ISSN: 1648-6897 / eISSN: 1822-4199

VILNIUS TECH
Vilnius Gediminas Technical University

JOURNAL of ENVIRONMENTAL ENGINEERING & LANDSCAPE MANAGEMENT

2026
Volume 34
Issue 4
Pages 406–419
https://doi.org/10.3846/jeelm.2026.26053

ANALYZING THE EFFECTIVENESS OF URBAN WATER BODIES IN MITIGATING URBAN HEAT ISLAND USING GEO-STATISTICAL METHODS

Nada Tarek ALI ABDALLA, Mohga Emam EMBABY, Ali Essam EL-SHAZLY

Department of Architecture, Faculty of Engineering, Fayoum University, Fayoum, Egypt

Highlights:

- urban water bodies reduce UHI, with smaller ones needing more research focus;
- larger water bodies cool more, but space efficiency matters in smaller areas;
- trees and land features enhance water bodies' role in UHI mitigation;
- multiple small lakes can outperform one large, irregular lake in cooling UHI.

Article History:

- received 25 January 2025
- accepted 26 January 2026

Abstract. Urban water bodies significantly contribute to mitigating the Urban Heat Island (UHI) effect, particularly during hot summer months. However, most studies have primarily focused on large water bodies, often overlooking the role and efficiency of smaller or medium-sized artificial ones. This study addresses this gap by examining the cooling performance of water bodies across different spatial contexts. While previous research has explored temperature reduction and cooling distances, key metrics such as cooling efficiency and the threshold value of efficiency remain underexplored, especially for smaller features. Moreover, recent findings suggest that cooling outcomes vary by climate, emphasizing the importance of climate-zone-specific investigations, particularly in hot arid regions, where cooling is closely linked to low humidity and high evapotranspiration. Effective landscape management can further enhance the arrangement of water bodies and surrounding land cover to mitigate the effects of climate change.

This research employs kernel density theory and geostatistical tools using Landsat 8 imagery, Python, R, ArcGIS, and SPSS to analyze the spatial decay of water-induced cooling. Regression analysis indicates that larger water bodies extend their cooling effect proportionally. However, in compact urban environments, optimal cooling may be achieved through strategically arranged smaller lakes or geometrically simple artificial water features. Integrating water bodies into broader urban ecosystems supports alignment with environmental sustainability goals.

Keywords: environmental sustainability, Urban Heat Island (UHI), Urban Heat Island Intensity (UHII), urban water bodies, cooling effect, Land Surface Temperature (LST), hot-arid climate, spatial analysis, landscape management.

Corresponding author. E-mail: *nt1116@fayoum.edu.eg*

1. Introduction

According to a report released by the United Nations, 55% of the global population lived in urban areas in 2018, a figure expected to rise to 68% by 2050 (United Nations, 2019). As a result, natural landscapes are increasingly being transformed into built environments to accommodate urban development, leading to a range of environmental and ecological challenges, chief among them the Urban Heat Island (UHI) effect, which poses significant environmental and public health risks (Luo & Lau, 2019). In addition, global climate change is increasing the frequency and intensity of extreme weather events, further exacerbating the UHI effect. This phenomenon intensifies energy and water demand, elevates carbon dioxide emissions, increases heat stress and air pollution, and ultimately undermines the health and comfort of urban populations (Yu et al., 2020; Sun & Chen, 2012). Although extreme storms often receive greater media attention, the National Oceanic and Atmospheric Administration (NOAA) reports that heat is typically more deadly than hurricanes and floods (Theeuwes et al., 2013).

The results of a recent study conducted in Melbourne, Australia (an urban environment without significant water bodies despite having green spaces) indicated that the Central Business District (CBD) and industrial suburbs retain the stored heat from the previous day until the following sunrise. This explains why urban areas remain warmer than surrounding suburban and rural zones (Luan et al., 2022). This is precisely the effect of urban heat islands, which occur due to two primary factors: first, buildings, roads, and paved surfaces store heat during the day and

Copyright © 2026 The Author(s). Published by Vilnius Gediminas Technical University

This is an Open Access article distributed under the terms of the Creative Commons Attribution License (*http://creativecommons.org/licenses/by/4.0/*), which permits unrestricted use, distribution, and reproduction in any medium, provided the original author and source are credited.

slowly release it during the evening. The second factor is attributed to anthropogenic heat emissions, including combustion processes from vehicles and industrial activities, as well as heat released from air-conditioning systems in residential and commercial buildings (United Nations, 2019).

One option for addressing urban heat islands is to implement green and blue infrastructure as part of urban design. This approach is widely recognized as one of the most effective strategies for mitigating and adapting to urban heat island effects. Blue infrastructure consists of water bodies in urban landscapes that play an active role in regulating the local microclimate (Eggimann et al., 2017).

Most current research emphasizes the impact of large-scale lakes, oceans, and rivers on urban heat islands, often overlooking the relationship between water bodies and UHI across different spatial scales. It is therefore important to compare water bodies of varying sizes within similar urban settings to establish a meaningful connection between UHI intensity and water body scale (Eggimann et al., 2017). However, due to variations in urban context and methodological approaches (e.g., LST inversion techniques and satellite image resolution), as well as seasonal and diurnal variability, considerable debate remains regarding the cooling effects of water bodies – particularly smaller or medium-sized features – which still require further clarification (Yu et al., 2020; Sun & Chen, 2012).

Several studies (e.g., Chang et al., 2007; Sun & Chen, 2012; Du et al., 2016) have proposed methods to quantify the temperature reduction and spatial extent of cooling effects from blue-green spaces. However, key concepts such as cooling efficiency and threshold value of efficiency remain underexplored. While recent works (e.g., Yu et al., 2017; Fan et al., 2019) have begun to define these metrics, findings remain inconsistent due to differences in urban and climatic contexts. Notably, studies like Zhao et al. (2014) highlighted that high cooling performance is often linked to low humidity and elevated evapotranspiration rates, reinforcing the importance of climate-zone-specific research.

In response to the aforementioned issues, this study examines the differences in the spatial extent and magnitude of the impact associated with water bodies of different sizes under similar climatic and urban conditions. The analysis aims to uncover the theoretical relationship between water-body cooling attenuation, water surface area, and Urban Heat Island Intensity (UHII) sensitivity. The study provides a scientific basis to support planners and architects in designing urban water bodies as an effective strategy to mitigate urban heat island effects. The added value of this research lies in quantifying the mathematical relationship between water surface area and its cooling impact range on UHII, with water body area considered as the independent variable and impact range as the dependent variable.

The unique feature of this study, which supports the formulation of the proposed relationship, is the analysis and comparison of data from 14 water bodies of varying sizes, located within a similar spatial, climatic, and environmental context in the New Cairo urban area. This approach allows the study to minimize the influence of external variables and focus specifically on the characteristics of water bodies and their impact on UHII.

This study is organized into four sections following this introduction. The first section provides background information on the UHI phenomenon and distinguishes between UHI and UHII, as well as explains how water bodies can mitigate UHI intensity. The second section describes the methods and materials used to conduct the applied study. In the third section, the results demonstrate that the influence of water body area on UHII should be carefully considered in urban design, as increasing the area may enhance cooling effects or, alternatively, lead to inefficient land use when no significant improvement is achieved. The final section presents the study's conclusions and highlights directions for future research.

Urban Heat Islands (UHI) are described by "Kevin Trenberth", a renowned climate scientist, as" regions within cities where temperatures significantly exceed those in the surrounding areas". This temperature disparity is primarily caused by human activities and urbanization, which significantly influence the local climate. This section examines the role of water bodies in moderating Urban Heat Island Intensity (UHII). UHII is defined as the temperature difference between urban areas, such as cities, and adjacent suburban or rural regions. It serves as a metric for quantifying the strength of UHI and is typically determined by comparing temperature measurements obtained from urban and suburban/rural locations (Oke, 2002). UHI refers to the phenomenon as a whole, whereas UHII denotes the measurable intensity of the phenomenon at a specific location. These heat islands contribute to excessive urban temperatures, adversely affecting public health and environmental sustainability in several ways. Such impacts include increased energy demand for air conditioning, degraded air and water quality, and alterations to the local climate.

Previous literature on UHI indicates that urbanization is a key contributor to the urban heat island effect, involving the conversion of natural landscapes into built environments characterized by impervious surfaces such as concrete and asphalt. Inadequate landscape management further intensifies this effect by reducing evapotranspiration from green and blue urban surfaces, thereby exacerbating the UHI phenomenon (Ballout et al., 2015; Estoque et al., 2017). Accordingly, the integrated use of green and blue infrastructure is recommended as part of future urban growth strategies, particularly in regions experiencing high summer temperatures and rapid urban expansion (Gunawardena et al., 2017).

Although water features are commonly used in urban planning as aesthetic elements for public spaces (Du et al., 2016), they can help mitigate the impact of urban heat islands in various ways. Water bodies cool nearby air by evaporation and act as thermal sinks, reducing the uptake of heat. This results in a reduction in the amount of heat absorbed by buildings, roads, and other urban surfaces.

Additionally, water bodies can contribute to improving air quality by helping reduce dust and unpleasant odors, thereby mitigating air pollution. Accordingly, the integration of water features into urban planning can enhance urban livability and reduce the impacts of urban heat islands. However, it is crucial to base the design of water features on comprehensive scientific studies to avoid disrupting the local climate, ecological balance, or inefficient use of urban space (Abrahem et al., 2022).

Research on the role of water features in mitigating Urban Heat Island (UHI) effects remains limited, partly because their climatic influence is often considered smaller than that of green areas. However, the growing demand to incorporate water bodies into urban projects makes it essential to assess their impact to optimize design potential (Imam Syafii et al., 2017). For example, Xu et al. (2010) examined the thermal comfort effects of water bodies during extremely hot days (air temperatures above 35 °C) using field observations.

Their findings indicate that water bodies larger than 2,104 m^2 significantly cool their surrounding areas. Similarly, a modeling study by Inard et al. (2004) demonstrated that even very small basins (4 m^2) can produce a cooling effect in their immediate surroundings. Furthermore, the spatial distribution of multiple small water bodies across an urban area can lead to a greater temperature reduction compared to a single water body of equivalent total volume (Gunawardena et al., 2017). The geometry of water features also influences the distribution of cooling effects. Studies by Gunawardena et al. (2017), Lee et al. (2016), and Mostofa and Manteghi (2019) indicate that simpler and more regular shapes provide higher cooling efficiency than irregular configurations.

Despite numerous scientific articles highlighting the advantage of water bodies as the best means of passive cooling, they may not work optimally in hot and humid regions. The evaporation from water features, such as artificial waterfalls and water curtains, if implemented in a warm and humid climate, may increase the humidity level beyond the comfort level (Wong et al., 2012).

Smaller water bodies, such as fountains and artificial ponds, require further investigation to accurately quantify their thermal effects. Most existing studies focus on a single water body, relying on either field observations or simulation-based approaches. In contrast, the present study adopts a comparative approach, examining multiple

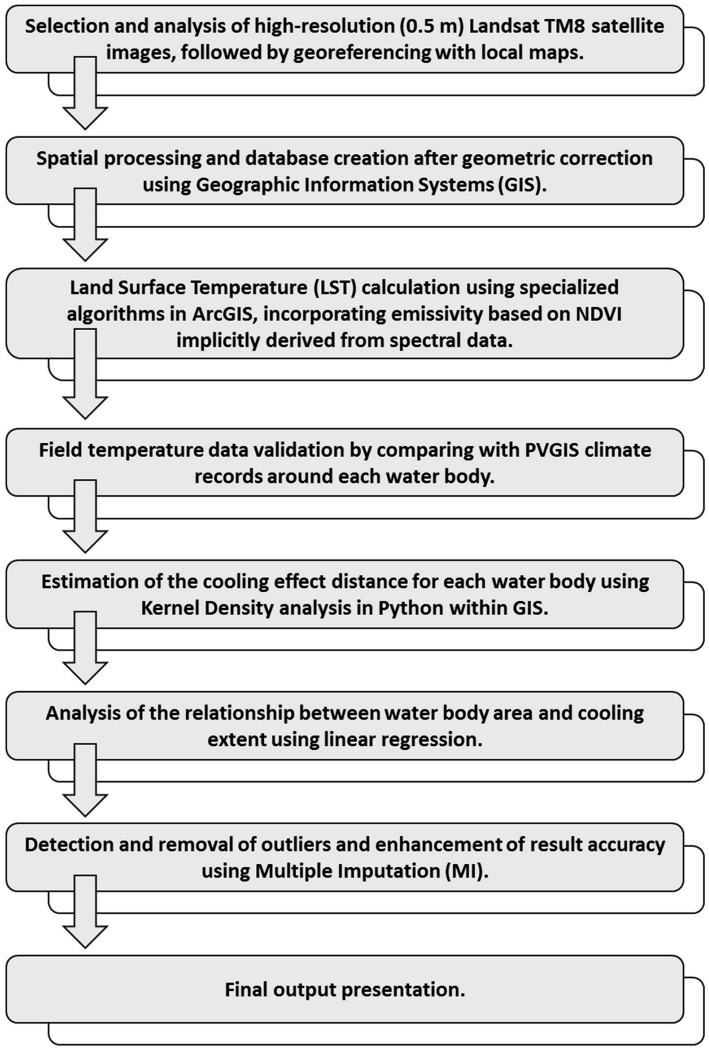


Figure 1. The adopted research methodology

geometrically similar industrial lakes of varying sizes under consistent climatic and urban conditions.

This section highlights that the UHI phenomenon represents a global challenge due to its association with climate change and how water bodies can mitigate its intensity. The following section explores the challenge of obtaining accurate information and results for the comparison process. The procedures and methods for this study are described below.

2. Methods and materials

To address the complex relationship between urban thermal behavior and the moderating effect of water bodies, a systematic and data-driven methodology was adopted. This methodology integrates spatial analysis, thermal data extraction, statistical modeling, and geospatial validation tools. The full workflow is illustrated in Figure 1, which outlines the sequential steps followed throughout the study. Landsat 8 satellite imagery was analyzed using Geographic Information Systems, where the images were imported into ArcGIS for georeferencing and layer preparation. Land Surface Temperature (LST) was calculated using Eq. (1) through Python scripting within the Raster Calculator tool in ArcGIS. After identifying the coordinates of a reference point in the suburbs, the Urban Heat Island Intensity (UHII) was calculated using Eq. (2). The spatial threshold of each water body's influence on UHII was then determined by applying Eq. (3) using Python within the Spatial Analyst tool in ArcGIS, based on Kernel Density analysis. A linear regression analysis was subsequently conducted using Eq. (4) in SPSS, which revealed anomalies in the sample series and a relationship between specific surface areas and their cooling effect. To identify and eliminate outliers, Eq. (5) was applied using SPSS as well. To enhance the reliability of the results, Multiple Imputation (MI) was employed using the "mice" package in R with Eq. (6), and the outputs were then integrated into SPSS for the final presentation and interpretation of results.

2.1. Case study

Cairo Governorate is subject to continuous urban growth driven by internal migration and urban expansion. It is the largest urban area in Egypt, Africa, and the Middle East, and the 17th largest city globally, with a population of approximately 21 million (Elmarakby et al., 2022). This study focuses on New Cairo City, located within Cairo Governorate, which was specifically selected as the case study due to its classification as a third-generation city that emphasizes technological integration to enhance quality of life and improve public services and infrastructure, thereby promoting greater urban comfort and efficiency. New Cairo is one of the largest new cities in Egypt, with an urban mass area of approximately 67,000 acres out of a total area of 85,000 acres. It comprises several residential communities, most notably the Fifth Settlement, in addition to Al Rehab, the First Settlement, the Third Settlement, and other districts (Hafez, 2017). New Cairo (30°00′–30°05′ N, 31°30′–31°35′ E) is a rapidly developing satellite city located east of Cairo. It falls within the hot desert climate zone (BWh) according to the Köppen–Geiger classification. The area is characterized by a long and intensely hot summer season, with peak temperatures frequently exceeding 40 °C, very low annual precipitation (~30 mm), and more than 3,500 hours of sunshine annually (Hamed et al., 2022). Prevailing northwesterly winds, combined with sparse vegetation cover, significantly contribute to pronounced Urban Heat Island (UHI) effects. Despite their limited presence, open water bodies have the potential to moderate local microclimates through evaporative cooling. The selection of New Cairo, with its hot–arid climate, enables a focused investigation into the cooling effects of water bodies during peak daytime heat conditions. As demonstrated by Hong et al. (2023), water-body cooling is most effective during daytime hours and varies across climatic regions; in dry environments, such as Xi'an, the cooling effect persists throughout the day, whereas in humid regions, such as Chengdu, nighttime warming has been observed. These findings underscore the importance of climatic context when assessing water-mediated thermal mitigation. Egypt's human-induced greenhouse gas emissions in 2018 amounted to 329,220 metric tons of carbon dioxide equivalent, according to the World Bank, representing an increase of 2.76% compared to 2017 (World Bank, n.d.). Cairo Governorate alone accounts for approximately 62% of national emissions, corresponding to about 0.7% of global emissions (Theeuwes et al., 2013). As a result, Cairo Governorate is increasingly exposed to extreme weather events, including heatwaves intensified by Urban Heat Island formation, as well as dust storms and flooding, particularly over the past decade. Scientific evidence indicates that both the frequency and intensity of these events are rising as a consequence of climate change. Moreover, Cairo Governorate is experiencing a growing demand for energy, further compounding these challenges (Jungudo, 2022).

The aforementioned factors highlight the need for studies that demonstrate solutions to mitigate the UHII in densely populated urban areas. The thermal map of Cairo Governorate revealed a distinctive thermal pattern associated with the UHII phenomenon. This thermal pattern was evident through a reduction in Land Surface Temperature (LST) in certain urban areas of New Cairo City, with the effect more pronounced in locations containing water bodies. Accordingly, sites featuring artificial lakes within social clubs were selected to isolate the cooling effects of water bodies from those of surrounding buildings and streets, and to enhance the reliability of the results by enabling the identification of consistent patterns and potential variations. Unlike public parks or mixed-use urban spaces, these sites offer controlled environments with minimal external interference, thereby reducing the influence of variables such as irregular human activity, temporary installations, or inconsistent vegetation management, all of which could otherwise introduce measurement bias.

A preliminary (LST) analysis was conducted to assess multiple potential sites. This initial screening confirmed that Katameya Dunes Golf & Social Club, Katameya Heights Golf Club, and Mirage City Executive Golf Course offer the most suitable conditions for isolating the thermal effects of water bodies from surrounding urban influences.

The three projects are, katameya dunes golf & social club, (Figure 2), katameya heights golf club, (Figure 3), and Mirage City Executive Golf Course, (Figure 4), contain a total of 14 water bodies with varying sizes, as shown in Table 1. These sites were deliberately selected to ensure that no major urban obstacles, such as high-rise buildings

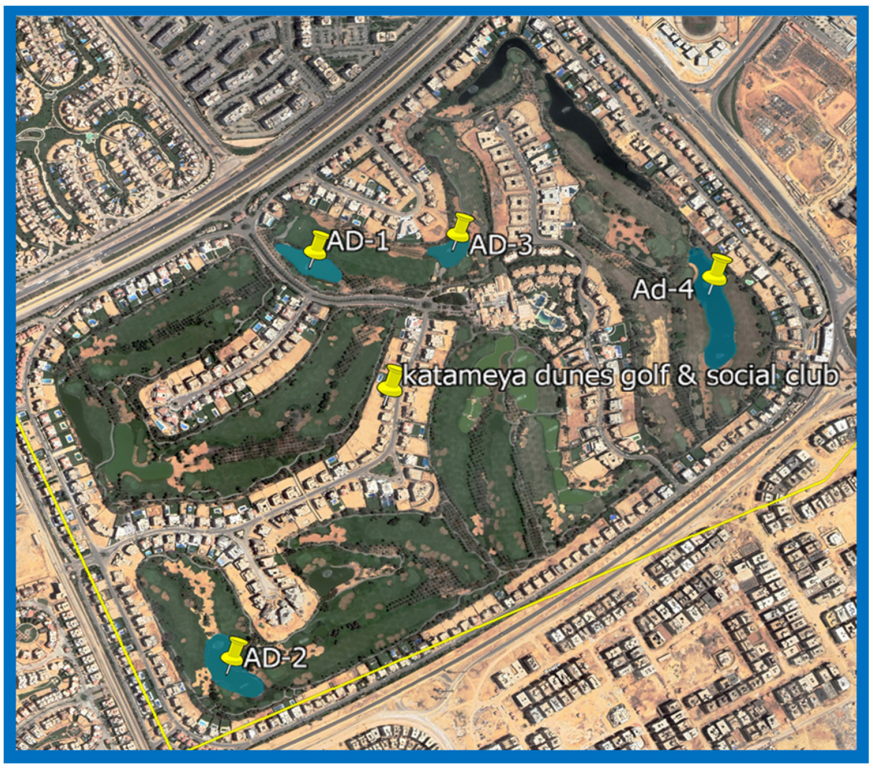


Figure 2. Katameya dunes golf & social club

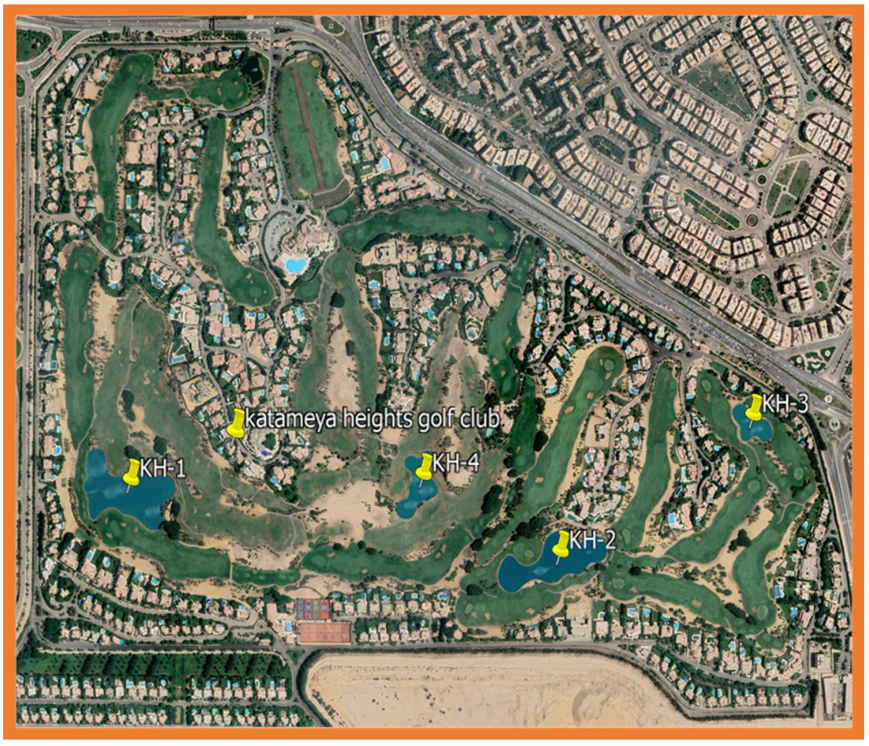


Figure 3. Katameya heights golf club

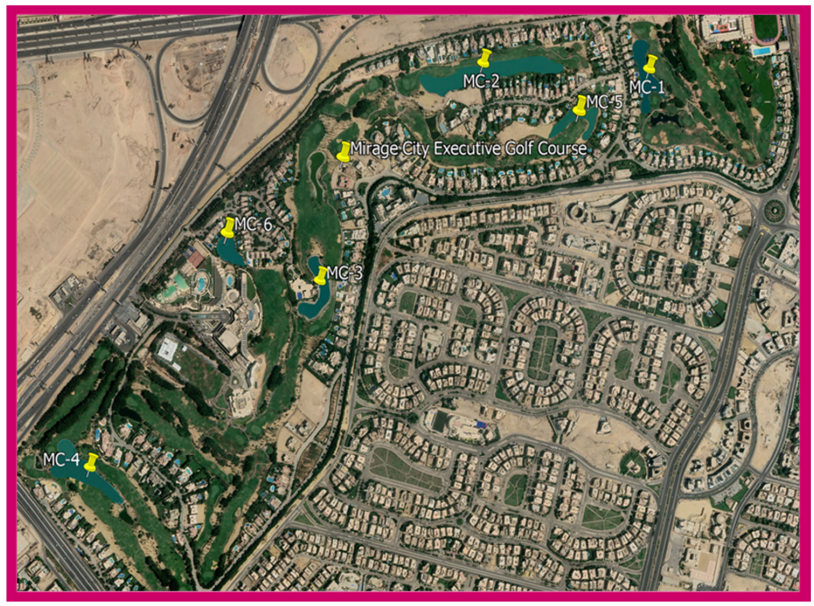
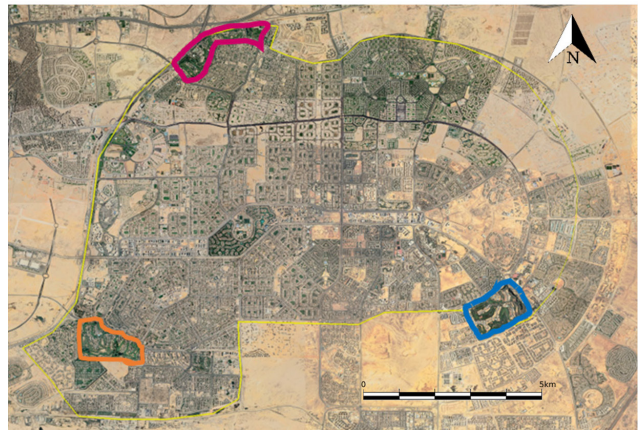
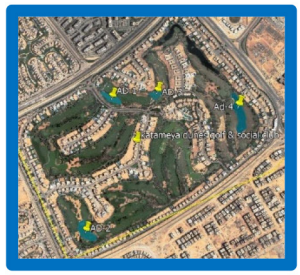
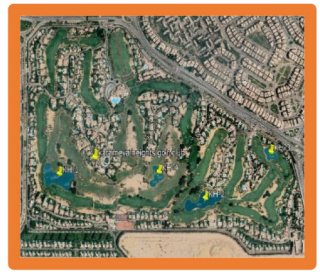
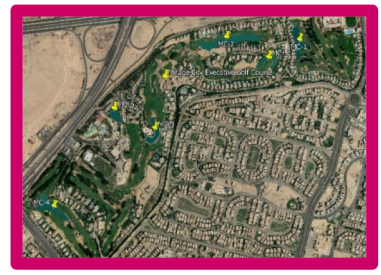


Figure 4. Mirage City Executive Golf Course

Table 1. The three locations of the study areas in New Cairo

New Cairo satellite image			
Study area satellite image	Katameya dunes golf & social club	Katameya heights golf club	Mirage City Executive Golf Course
			
Coordinates	30° 0′14.70″N AD-1 31°31′3.21″E 29°59′44.32″N AD-2 31°30′56.34″E 30° 0′15.92″N AD-3 31°31′14.52″E 30° 0′12.43″N AD-4 31°31′34.72″E	29°59′28.00″N KH-1 31°24′4.80″E 29°59′23.19″N KH-2 31°24′40.01″E 29°59′31.49″N KH-3 31°24′55.96″E 29°59′28.10″N KH-4 31°24′28.84″E	30° 4′40.02″N MC-1 31°26′51.43″E 30° 4′40.80″N MC-2 31°26′32.39″E 30° 4′21.29″N MC-3 31°26′13.33″E 30° 4′4.73″N MC-4 31°25′46.64″E 30° 4′34.85″N MC-5 31°26′42.53″E 30° 4′24.55″N MC-6 31°26′3.09″E

or dense street networks, obstruct the influence radius of the water bodies, thereby enabling a more accurate assessment of their maximum cooling potential. Despite the existence of numerous water bodies in modern residential complexes in New Cairo city, these particular sites were chosen specifically to avoid building interference in the measurement process, to determine the maximum extent to which the water body's effect on UHII can be reached without being obstructed by a building or any other urban obstacle that affects the analysis process.

2.2. Remote sensing technology

UHII is measured at the local scale using remote sensing techniques based on LST retrieval and a spatial distribution procedure for UHII. LST is calculated using the following equation:

$$LST = \frac{BT}{\left[1+\left(\left(\frac{\lambda * BT}{C}\right)\ln(e)\right)\right]}, \quad (1)$$

where BT = average brightness temperature; λ = Landsat 10 band of Landsat visuals, C = 14388 mK, e is the emissivity (Elmarakby et al., 2022). In this study, e was derived based on NDVI thresholds, following the method proposed by (Sobrino et al., 2004), to improve LST retrieval accuracy across different land cover types.

2.3. UHII calculation method

As mentioned earlier, the difference between urban area temperature and suburban temperature is defined as UHII. UHII can be calculated by finding the difference in temperature between a spatial location in the city and the suburbs at a given time. The calculation equation is:

$$\Delta T_{ij} = T_{ij} - T_R, \quad (2)$$

where ΔT_{ij} is the UHII at the spatial location ij, T_{ij} is the surface temperature at the location, and T_R is the suburban temperature (Oke, 2002). In this study, UHII was estimated based on LST data, using suburban LST as the reference temperature (TR) for comparison with urban values.

2.4. Kernel density estimation

Density is a field expression of spatial void. It is determined by the relationship between adjacent spatial locations. It is computational counterpart is based on the first law of geography, which assumes that adjacent points or samples are closely related in properties. In this study, the kernel density bandwidth parameter (h) was empirically determined through repeated experimental trials using observed and corrected temperature data from multiple sampling points surrounding the water bodies, with different bandwidth values tested to ensure spatial consistency and minimize estimation error; accordingly, kernel density estimation was selected over alternative approaches such as fixed buffer analysis or distance-based decay models due to its ability to capture the continuous spatial attenuation of cooling effects without imposing rigid distance thresholds. As a highly reliable analysis tool, the kernel density method can check the spatial distribution properties that are clustered or symmetrical, which enables us to use it in the analysis process (Borruso, 2003). The principle of the kernel density estimation method is to take X as the center of the circle and the threshold value h as the radius to sum the number of information variables in the circle composed of X and h and divide the number by the area of a circle. Kernel density at point X is calculated by the following equation:

$$\hat{f}_h(x) = \frac{1}{nh}\sum_{i-1}^{n} k\left(\frac{x - x_j}{h}\right), \quad (3)$$

where n is the number of observations within the distance scale; K is the kernel density function; h is the bandwidth (radius), which defines the scale of the kernel density estimation; and x and x_i are the estimation points, representing the Euclidean distance between the center point and any other point within the threshold. The bandwidth parameter (h) is the most critical component of the function, as it determines the appropriate spatial range of influence (Huang et al., 2017).

A kernel function is commonly applied to datasets that are not linearly separable in their original dimensional space, such as two-dimensional data where one data cluster is enclosed within another. In such cases, the kernel function implicitly projects the data into a higher-dimensional space, allowing linear separation through a hyperplane. Commonly used kernel functions include linear, polynomial, Radial Basis Function (RBF), and Gaussian kernels.

2.5. Correlation coefficient

The Pearson correlation coefficient is a measure of the linear relationship between two pairs of quantitative variables. It represents the ability to predict the value of a variable from the value of another variable. The Pearson correlation coefficient is calculated using the following equation:

$$s = \sum_{i=1}^{n}\left|\frac{\sum_{i=1}^{n}\left(x_i - \bar{x}\right)\left(y_i - \bar{y}\right)}{\sqrt{\sum_{i=1}^{n}\left(x_i - \bar{x}\right)^2}\sqrt{\sum_{i=1}^{\eta}\left(y_i - \bar{y}\right)^2}}\right|, \quad (4)$$

where S is the correlation coefficient between variables, x_i is the value of variable x of sample i, $\bar{x}$ is the arithmetic Mean of the values of variable x in the sample, y_i is the value of variable y of the sample i, $\bar{y}$ is the arithmetic Mean of the values of variable y in the sample. The Pearson correlation coefficient can be used in a predictive form to predict the value of one variable from the value of another variable, using the equation of the line representing the relationship between the variables. This equation is calculated

using the linear regression technique, and is determined by the known values of each of the variables and the Pearson correlation coefficient. Using this equation, the value of a variable can be predicted by entering the value of the other variable into the equation (Huang et al., 2017).

2.6. Detecting outliers using modified Z-score

In this method, we use the Median because it is not affected by outliers instead of the arithmetic mean that is affected by outliers, and we also use the Deviation from the Median and not the usual standard deviation from the arithmetic Mean.

$$M_i = \frac{0.6745(x_i - \tilde{x})}{MAD}, \quad (5)$$

$\tilde{x}$, which is the median of the sample, *MAD* the median of the absolute difference between each point and the median, M_i is Modified Z-score, and 0.6745 is the 0.75th quartile of the standard normal distribution. After calculating M_i for all sample values, any observation with an absolute modified Z-score greater than 3.5 (i.e., $|M_i| > 3.5$) is considered an outlier, following the standard threshold recommended by Iglewicz and Hoaglin (1993).

2.7. Regression with Multiple Imputation (MI)

The current view is that multiple imputation by chained equations data package (mice) In the R programming language is one of the best ways for missing data handling in regression, employing Predictive Mean Matching (PMM) as the imputation method. This approach is particularly suitable for continuous variables with non-normal distributions. The statistics of interest (for example, regression coefficients and their standard errors) are extracted from the analysis performed in each of the M computed datasets. In this study, multiple imputation using 5 chained equations (M = 5) was performed. Prior to imputation, all variables were examined for missingness patterns, and auxiliary variables correlated with the incomplete variables were included in the imputation model to improve estimation accuracy. Categorical variables were imputed using appropriate factor-level methods, while continuous variables were handled using PMM. Convergence of the chained equations was monitored through diagnostic plots to ensure stability of the imputations. Rubin's rules were then applied, and the coefficients and standard errors from each dataset were pooled to obtain the final estimates. Rubin's rules combine the estimates and standard errors across the computed datasets, whereby the estimate of the MI for the statistic is simply the average value of a statistic estimated across M computed datasets. The MI estimate of θ variance obtained using Rubin's rules is:

$$\text{var}(\theta) = w + \left[1 + \frac{1}{M}\right] B. \quad (6)$$

This quantity reflects both the mean within-embedding variance and the mean between-embedding variance in θ. where *w* is the mean of the estimated variance of a statistic estimated across *M* computed data sets, and *B* is the degree to which the estimated statistic varies across *M* computed data sets. Note that when single modulation is used, there is no estimate of B, so we cannot estimate true variance in the statistic (Austin et al., 2021).

3. Results of the research

According to the aforementioned data selection criteria, the Landsat 8 TM image acquired on 27 July 2022 was selected, as it exhibited minimal cloud cover (2.87%). For water-body data extraction, high-resolution OLI_TIRS

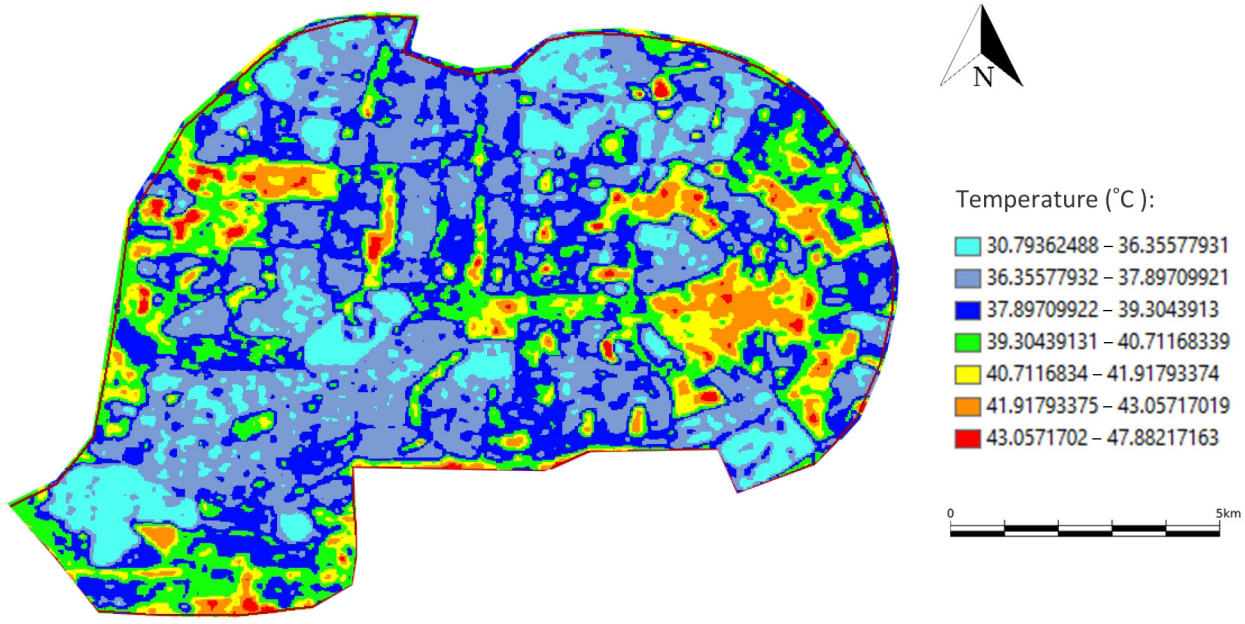


Figure 5. The results from analyzing the thermal pattern of the study area using remote sensing

imagery (spatial resolution: 0.5 m), acquired under WRS Path/Row 176/39, was used. These images were matched with a 1:2000 local area map and the overall New Cairo urban planning map. After geometric correction, the imagery and cartographic data were uniformly projected to WGS_1984_UTM_Zone_36N, and a Geographic Information System (GIS) database was established. Following layer preparation, Land Surface Temperature (LST) was calculated for the study area. Thermal analysis of the case studies showed that the maximum UHI value reached 47.88 °C, while the maximum UHII value was 2.26, and the minimum UHII value was 8.92 (Figure 5).

Data was compared and corrected with climate data sets from PVGIS for temperature at 30 selected points around each one of the 14 water bodies in each of the three projects. Although formal cross-validation techniques were not applied, the bandwidth was not arbitrarily selected. It was empirically derived through repeated experimental trials using observed and corrected temperature data from various point groups around the water bodies, analyzed across multiple time intervals. The total error was controlled within 15 m. the temperature measures were conducted at 30 min intervals. the observed temperature error was ± 0.3 °C. to comply with the ArcGIS requirements of spatial uniformity and rational distribution of sample data, the measured temperatures were between 8am and 5pm, and it was observed that the effect of water bodies on reducing UHII was strongest between 1pm and 2pm, where the correlation coefficients obtained exceeded the confidence level of 0.05. Consequently, the measurement time for all study points was standardized at 2pm.

By applying Eq. (3) using Python programming language in GIS, the program allowed us to access the distance threshold value (Table 2) for each water body, which in this case represents the extent of the water body's effect on UHII.

After measuring the area of each water body and extracting the range by applying the nucleus density equation to the 14th study sample, linear regression was applied to the results and from observations, anomalies were found in the sequence of sample values, in addition to the existence of a relationship between specific areas and their impact (Figure 7).

To identify and remove outliers in the samples, Eq. (5) was used and applied to the data using SPSS software. Outliers were detected in the data, as shown in Table 2, and upon reviewing the reasons for these outliers, it was found that the presence of trees within the original range of water bodies impact increases the range on UHII, while the presence of non-cultivated or sandy areas within the range reduces the range of the water surface impact on UHII.

Referring back to Figure 7, the points on the regression line were divided into three groups, as shown in the figure. To study the case better, the research proposed the Multiple Imputation (MI) theory using the mice package in R for analyzing datasets with missing values in the regression. To address missing data, five imputations (M = 5)

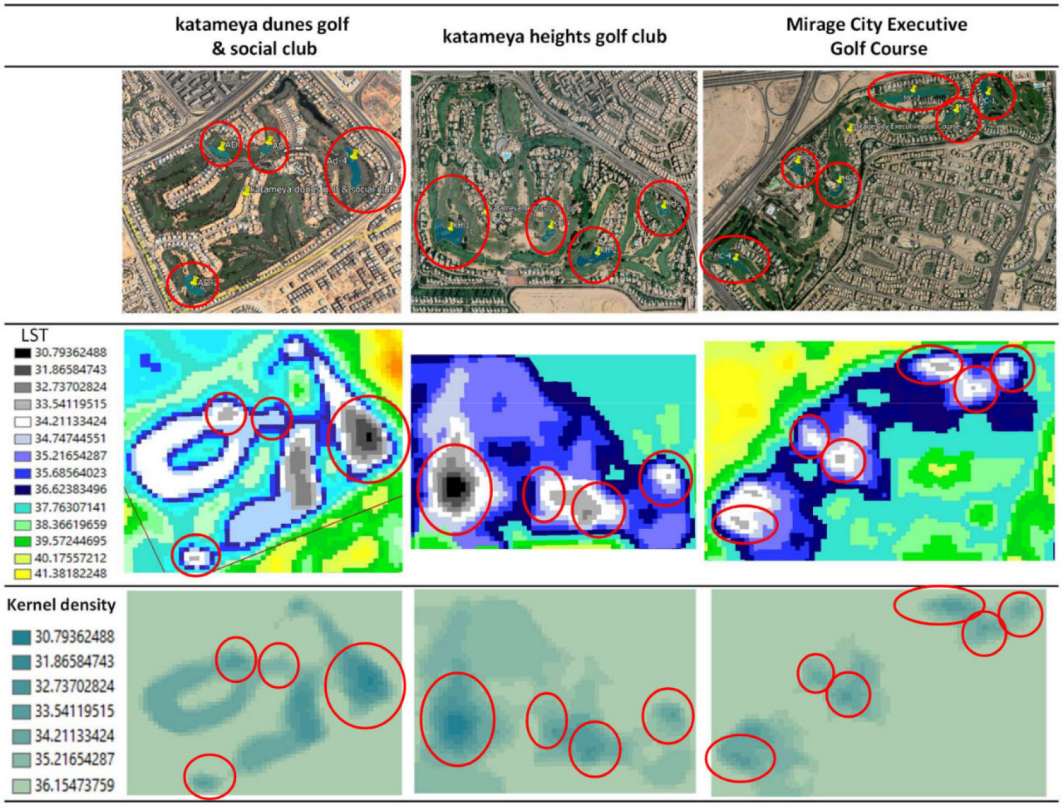


Figure 6. The results from analyzing the LST and the Kernel Density on the local scale using remote sensing and Python programming language

were generated, in line with common recommendations in the literature for datasets with moderate levels of missingness. Eq. (6) was applied in the R programming interface, and the results were integrated into SPSS for visualization. The analysis revealed a gap in the range of spheres of influence, indicating that, 1) the linear equation of the water bodies impact range (C) between 3000 ≥ 7000 is Y = –0.156 + 0.003X and the error factor is ±0.967. This implies that in this area, the range of water bodies impact increases by a distance of 1 meter for every 368 m2 increase in the water body area. 2) The linear equation of the water bodies impact range (B) between 7500 ≥ 14000 is Y = 0.517 + 0.005X and the error factor is ±1.736, which means that in this area, the range of water bodies impact increases by a distance of 1 meter for every 184 m2 increase in the water body area. 3) The linear equation of the water bodies impact range (A) between 14300 ≥ 18000 is Y = –0.552 + 0.008X and the error factor is ±2.921, meaning that in this area, the range of water bodies impact increases by a distance of 1 meter for every 127 m2 increase

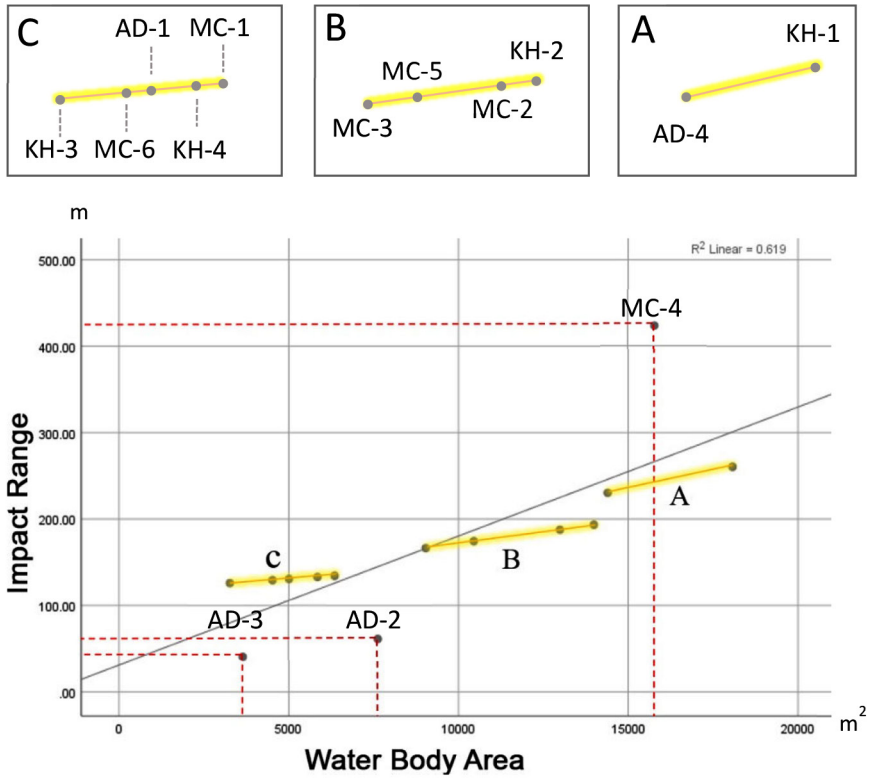


Figure 7. Water Body Area and Impact Range correlation in the 14 artificial lakes

Table 2. Outlier data in the study samples and the reason for its anomaly

GROUP	LAKE	AREA (m^2)	RANGE (m)	UHII (°C)	REMARKS
A	KH-1	18072	260.43	2.26	
	MC-4	15783	423.29	6.37	A line of trees around it
	AD-4	14395	230.35	2.94	
B	KH-2	13987	193.43	3.71	
	MC-2	12987	187.58	3.72	
	MC-5	10451	174.42	4.63	
	MC-3	9035	166.37	4.61	
	AD-2	7636	61.33	8.35	uncultivated areas around it
C	MC-1	6351	134.31	5.43	
	KH-4	5845	132.88	5.74	
	AD-1	5007	130.64	6.93	
	MC-6	4520	129.28	7.06	
	AD-3	3657	40.66	8.92	uncultivated areas around it
	KH-3	3265	125.87	7.44	

in the water body area, where Y in the three groups represents the extent of UHII influence and the X represents the area of the water body. The three aforementioned points are clear in Figure 8, where the first figure on the left (Figure 8a) represents all the points collected, while (Figure 8b, c, d) represent each group of similar areas in terms of characteristics individually (A, B, C). Linear regression models were applied separately for the three groups (A, B, and C) based on the water body area ranges. The R^2 values were 0.995 for group (A), 0.958 for group (B), and 0.956 for group (C), indicating strong positive relationships between water body area and cooling impact range. All models were statistically significant (p-values < 0.00001). The 95% confidence intervals for the slope coefficients were as follows: group (A) [0.0062, 0.0098], group (B) [0.0044, 0.0056], and group (C) [0.0025, 0.0035].

Based on the analysis of this study, it is evident that larger water bodies (Group A) tend to exhibit a wider spatial extent of cooling, yet the actual reduction in UHII is relatively modest. In contrast, smaller water bodies (Group C), although their spatial cooling range is limited, demonstrate a more significant temperature drop in their immediate surroundings.

This discrepancy can be partially attributed to the thermal properties of water. When a water body is large, such as a sea or a deep lake, it possesses a high thermal mass, allowing it to store heat for extended periods. As a result, nighttime radiative heat release from the water surface can maintain elevated air temperatures in adjacent areas, thereby reducing the net nighttime cooling effect. Conversely, smaller and shallower water bodies tend to dissipate heat more rapidly due to their lower volume and depth, enabling them to cool the surrounding air more effectively at night, particularly under conditions of enhanced evaporative cooling.

Grass enhances the impact, while asphalt or non-cultivated areas reduce the impact and may even cancel it altogether. When two artificial lakes are located in close proximity, a cool air corridor can form between them (Table 2) as a result of the displacement of warmer, less dense air by cooler air masses. Accordingly, this mechanism suggests that, in certain urban projects, the design of multiple smaller lakes may be more effective than a single large water body. Furthermore, simpler or more regular shapes of artificial lakes provide higher efficiency compared to irregular shapes.

Therefore, the study not only compares thermal performance across water body sizes but also highlights the nonlinear relationship between size, thermal inertia, and cooling efficiency. This refined understanding suggests that cooling performance is not strictly proportional to water-body area and that oversizing water features may result in inefficient land use without delivering substantial thermal benefits.

4. Discussion

The study aimed to enhance understanding of the role of water bodies in mitigating Urban Heat Island Intensity (UHII) through a comparative analytical approach. By integrating high-resolution Landsat imagery, PVGIS climatic data, and advanced spatial analysis techniques, this research provides novel insights into how variations in water-body area influence urban cooling.

It should be noted that the cooling performance of urban water bodies may vary depending on climatic

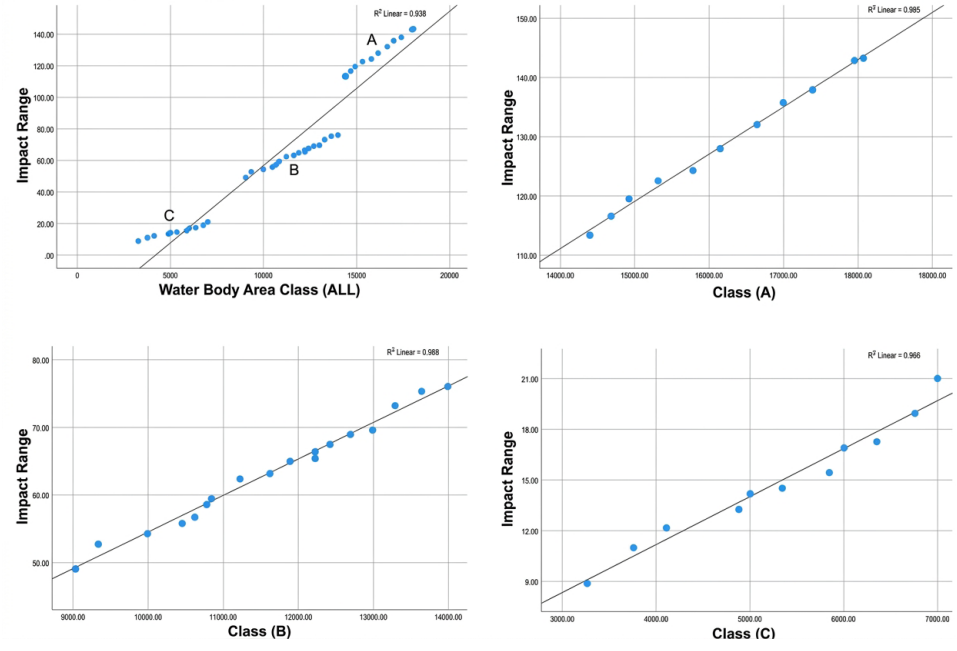


Figure 8. Correlation between Class (ALL, A, B, C) and the impact range: a) (ALL) Class and impact range correlation; b) Class ((A) between 14300 ≥ 18000m^2) and impact range correlation; c) Class ((B) between 7500 ≥ 14000m^2) and impact Range correlation; d) Class ((C) between 3000 ≥ 7000m^2) and impact range correlation

conditions. In hot–arid climates, such as New Cairo, evaporative cooling tends to be more effective due to low humidity levels, whereas in humid climates – as confirmed by previous studies – limited evaporative potential and elevated atmospheric moisture may reduce cooling intensity and alter the spatial extent of its influence. Moreover, evaporation from water features such as artificial waterfalls and water curtains, when implemented in warm and humid climates, may increase ambient humidity beyond thermal comfort thresholds.

4.1. Influence of water bodies on UHII mitigation

The final model demonstrated a significant and positive relationship between water body area and its cooling effect on UHII, supporting the hypothesis that increasing water body size enhances its impact on local temperature reduction. This aligns with findings from (Xu et al., 2010), who observed that water bodies larger than 2,104 m^2 significantly lowered surrounding temperatures. Similarly, (Inard et al., 2004) confirmed that even small basins (4 m^2) contribute to localized cooling. However, our study refined this understanding by establishing a quantitative relationship, where each additional square meter of water body area extends the cooling effect by approximately one meter, contingent on spatial classification (A, B, C). This finding underscores the necessity for optimized water body sizing in urban planning to maximize thermal benefits.

Contrary to previous studies that focused on individual water features, such as fountains and ponds (Wong et al., 2012), our study employed a multiple-area comparison approach, providing a broader perspective on the cumulative cooling effects of strategically distributed water bodies. In doing so, our results revealed a steeper cooling gradient than that reported by Gunawardena et al. (2017), who observed a 0.5 °C decrease with a 500 m^2 water body. The results support (Gunawardena et al., 2017), who emphasized the advantage of multiple small water bodies over a single large water feature for achieving widespread cooling effects in urban environments.

4.2. The role of landscape management and design considerations

The study further revealed that tree cover and surrounding land use significantly enhanced the cooling potential of water bodies, reinforcing findings from (Ballout et al., 2015; Estoque et al., 2017) , which highlighted the role of evapotranspiration in mitigating UHII effects. This suggests that integrating water features with vegetative landscapes amplifies their cooling efficiency, an aspect often overlooked in conventional urban design strategies.

Regarding shape efficiency, our results align with research by Gunawardena et al. (2017), Lee et al. (2016), and Mostofa and Manteghi (2019), which found that simpler or more regular-shaped water bodies offer greater cooling efficiency than irregular ones. The findings suggest that urban planners should prioritize geometrically optimized water features to maximize temperature reduction effects while minimizing spatial inefficiencies.

4.3. Implications for urban planning and future research

By integrating kernel density analysis and Multiple Imputation (MI) techniques, this study underscores the value of data-driven approaches in landscape planning for climate adaptation. The findings reinforce the importance of sustainable landscape management, aligning with Gunawardena et al. (2017), who emphasized the synergy of green and blue infrastructure for urban cooling. While NDVI was inherently used in the derivation of LST, it was not explicitly analyzed in isolation; future research should employ normalized NDVI metrics to quantify the contribution of vegetation to cooling efficiency.

While previous literature has primarily focused on qualitative assessments or limited case studies, this study bridges a critical research gap by offering a comparative, large-scale analysis. However, future research should explore the interplay between water body evaporation rates and regional humidity levels, particularly in hot and humid climates, as suggested by Wong et al. (2012), to ensure that cooling benefits outweigh potential drawbacks.

5. Conclusions

This study analyzed the impact of 14 water bodies in New Cairo on reducing Urban Heat Island Intensity (UHII), finding that cooling effects were most pronounced between 1 pm and 2 pm. Larger water bodies (Group A) exhibited a wider cooling extent but more modest temperature reductions, while smaller water bodies (Group C) provided stronger localized cooling within a shorter range. The relationship between water body area and UHII mitigation was found to be nonlinear, with diminishing returns for oversized features.

These findings can guide urban planners, landscape architects, and policymakers in optimizing the size, number, and placement of water features in hot-arid climates. For example, multiple small lakes or simpler, more regular shapes may deliver higher cooling efficiency than one large irregular feature. Integrating vegetation or shading around water bodies can further enhance their cooling potential.

The study's scope was limited by its reliance on single-season, daytime (summer) thermal conditions, in addition to the absence of wind speed, humidity, and seasonal or nighttime temperature variation data, which could influence cooling dynamics. In addition, results were based on conditions specific to New Cairo's urban form and climate, which may limit generalization to other contexts.

Future research should incorporate seasonal and diurnal data, in addition to meteorological parameters such as wind and humidity, to further refine the predictive models developed in this study. Expanding the scope of

analysis to include diverse climatic conditions and urban morphologies-particularly those dominated by high-rise buildings, where shading effects, urban canyon geometry, and altered wind regimes may significantly influence cooling performance and spatial extent of urban water bodies-would enhance the applicability of the proposed attenuation laws and regression-based thresholds in global urban design practice.

References

Abrahem, S. A., Taha, H., & Hassan, S. A. (2022). Effect of water features on the microclimate of residential projects in a hot-arid climate. *Acta Scientiarum Polonorum Administratio Locorum*, *21*(3), 5–13.

Austin, P. C., White, I. R., Le, D. S., & van Buuren, S. (2021). Missing data in clinical research: A tutorial on multiple imputation. *Canadian Journal of Cardiology*, *37*(9), 1322–1331. https://doi.org/10.1016/j.cjca.2020.11.010

Ballout, A., Lacheheb, D. E. Z., & Bouchahm, Y. (2015). Improvement of thermal comfort conditions in an urban space (Case study: The Square of Independence, Sétif, Algeria). *European Journal of Sustainable Development*, *4*(2), 407–418.

Chang, C.-R., Li, M.-H., & Chang, S.-D. (2007). A preliminary study on the local cool-island intensity of Taipei City parks. *Landscape and Urban Planning*, *80*(4), 386–395. https://doi.org/10.1016/j.landurbplan.2006.09.005

Iglewicz, B., & Hoaglin, D. C. (1993). *How to detect and handle outliers* (Vol. 16). ASQ Press.

Borruso, G. (2003). Network density and the delimitation of urban areas. *Transactions in GIS*, *7*(2), 177–191. https://doi.org/10.1111/1467-9671.00139

Du, H., Xuejun, S., Hong, J., Zenghui, K., Zhibao, W., & Yongli, C. (2016). Research on the cooling island effects of water body: A case study of Shanghai, China. *Ecological Indicators*, *67*, 31–38. https://doi.org/10.1016/j.ecolind.2016.02.040

Eggimann, S., Mutzner, L., Wani, O., Schneider, M. Y., Spuhler, D., Moy de Vitry, M., Beutler, P., & Maurer, M. (2017). The potential of knowing more: A review of data-driven urban water management. *Environmental Science & Technology*, *51*(5), 2538–2553. https://doi.org/10.1021/acs.est.6b04267

Elmarakby, E., Khalifa, M., Elshater, A., & Afifi, S. (2022). Tailored methods for mapping urban heat islands in Greater Cairo Region. *Ain Shams Engineering Journal*, *13*(2), Aticle 101545. https://doi.org/10.1016/j.asej.2021.06.030

Estoque, R. C., Murayama, Y., & Myint, S. W. (2017). Effects of landscape composition and pattern on land surface temperature: An urban heat island study in the megacities of Southeast Asia. *Science of the Total Environment*, *577*, 349–359. https://doi.org/10.1016/j.scitotenv.2016.10.195

Fan, H., Yu, Z., Yang, G., Liu, T. Y., Liu, T. Y., Hung, C. H., & Vejre, H. (2019). How to cool hot-humid (Asian) cities with urban trees? An optimal landscape size perspective. *Agricultural and Forest Meteorology*, *265*, 338–348. https://doi.org/10.1016/j.agrformet.2018.11.027

Gunawardena, K. R., Wells, M. J., & Kershaw, T. (2017). Utilizing green and blue space to mitigate urban heat island intensity. *Science of the Total Environment*, *584–585*, 1040–1055. https://doi.org/10.1016/j.scitotenv.2017.01.158

Hafez, R. M. (2017). New cities between sustainability and real estate investment: A case study of New Cairo city. *HBRC Journal*, *13*(1), 89–97. https://doi.org/10.1016/j.hbrcj.2015.03.001

Hamed, M. M., Nashwan, M. S., & Shahid, S. (2022). Climatic zonation of Egypt based on high-resolution dataset using image clustering technique. *Progress in Earth and Planetary Science*, *9*, Article 35. https://doi.org/10.1186/s40645-022-00494-3

Hong, C., Qu, Z., Xu, W., & Gu, Z. (2023). Study on water cooling island effects under different climatic conditions. *City and Built Environment*, *1*, Article 4. https://doi.org/10.1007/s44213-022-00004-7

Huang, H., Yun, Y., Xu, J., Wang, S., Zheng, X., Fu, J., & Bao, L. (2017). Scale and attenuation of water bodies on urban heat islands. *Open House International*, *42*(3), 108–111. https://doi.org/10.1108/OHI-03-2017-B0022

Imam Syafii, N., Ichinose, M., Kumakura, E., Jusuf, S. K., Chigusa, K., & Wong, N. H. (2017). Thermal environment assessment around bodies of water in urban canyons: A scale model study. *Sustainable Cities and Society*, *34*, 79–89. https://doi.org/10.1016/j.scs.2017.06.012

Inard, C., Groleau, D., & Musy, M. (2004). Energy balance study of water ponds and its influence on building energy consumption. *Building Services Engineering Research and Technology*, *25*(3), 171–182. https://doi.org/10.1191/0143624404bt106oa

Jungudo, M. M. (2022). The impact of climate change in Egypt. *International Journal of Research*, *9*(3), 274–290.

Lee, D., Oh, K., & Seo, J. (2016). An analysis of urban cooling island (UCI) effects by water spaces applying UCI indices. *Journal of the Korean Society of Civil Engineers*, *7*(11), 810–815. https://doi.org/10.18178/ijesd.2016.7.11.886

Luan, Q., Cao, Q., Huang, L., Liu, Y., & Wang, F. (2022). Identification of the urban dry islands effect in Beijing: Evidence from satellite and ground observations. *Remote Sensing*, *14*(4), Article 809. https://doi.org/10.3390/rs14040809

Luo, M., & Lau, N.-C. (2019). Urban expansion and drying climate in an urban agglomeration of East China. *Geophysical Research Letters*, *46*(12), 6868–6877. https://doi.org/10.1029/2019GL082736

Mostofa, T., & Manteghi, G. (2019). Influential factors of water body to enhance the urban cooling islands (UCIs): A review. *International Transaction Journal of Engineering, Management, & Applied Sciences & Technologies*, *11*(2), 1–12.

Oke, T. R. (2002). *Boundary layer climates* (2nd ed.). Routledge. https://doi.org/10.4324/9780203407219

Sobrino, J. A., Jiménez-Muñoz, J. C., & Paolini, L. (2004). Land surface temperature retrieval from LANDSAT TM 5. *Remote Sensing of Environment*, *90*(4), 434–440. https://doi.org/10.1016/j.rse.2004.02.003

Sun, R., & Chen, L. (2012). How can urban water bodies be designed for climate adaptation? *Landscape and Urban Planning*, *105*(1–2), 27–33. https://doi.org/10.1016/j.landurbplan.2011.11.018

Theeuwes, N. E., Solcerová, A., & Steeneveld, G. J. (2013). Modeling the influence of open water surfaces on the summertime temperature and thermal comfort in the city. *Journal of Geophysical Research: Atmospheres*, *118*(16), 8881–8896. https://doi.org/10.1002/jgrd.50704

United Nations. (2019). *World Urbanization Prospects: The 2018 Revision*. https://doi.org/10.18356/b9e995fe-en

World Bank. (n.d.). *Metadata glossary*. https://databank.worldbank.org/metadataglossary/world-development-indicators/series/EN.ATM.GHGT.KT.CE?utm_source=chatgpt.com

Wong, N. H., Tan, C. L., Nindyani, A. D. S., Jusuf, S. K., & Tan, E. (2012). Influence of water bodies on outdoor air temperature in hot and humid climate. *ICSDC 2011: Integrating Sustainability Practices in the Construction Industry*, 81–89. https://doi.org/10.1061/41204(426)11

Xu, J., Wei, Q., Huang, X., Zhu, X., & Li, G. (2010). Evaluation of human thermal comfort near urban waterbody during summer. *Building and Environment*, *45*(4), 1072–1080. https://doi.org/10.1016/j.buildenv.2009.10.025

Yu, Z., Guo, X., Jørgensen, G., & Vejre, H. (2017). How can urban green spaces be planned for climate adaptation in subtropical cities? *Ecological Indicators*, *82*, 152–162. https://doi.org/10.1016/j.ecolind.2017.07.002

Yu, Z., Yang, G., Zuo, S., Jørgensen, G., Koga, M., & Vejre, H. (2020). Critical review on the cooling effect of urban blue-green space: A threshold-size perspective. *Urban Forestry & Urban Greening*, *49*, Article 126630. https://doi.org/10.1016/j.ufug.2020.126630

Zhao, L., Lee, X., Smith, R., & Oleson, K. (2014). Strong contributions of local background climate to urban heat islands. *Nature*, *511*, 216–219. https://doi.org/10.1038/nature13462